

A Practical Compressed Sensing-Based Pan-Sharpener Method

Cheng Jiang, Hongyan Zhang, Huanfeng Shen, and Liangpei Zhang

Abstract—High-resolution multispectral (HRM) images are widely used in many remote sensing applications. Using the pan-sharpening technique, a low-resolution multispectral (LRM) image and a high-resolution panchromatic (HRP) image can be fused to an HRM image. This letter proposes a new compressed sensing (CS)-based pan-sharpening method which views the image observation model as a measurement process in the CS theory and constructs a joint dictionary from LRM and HRP images in which the HRM is sparse. The novel joint dictionary makes the method practical in fusing real remote sensing images, and a tradeoff parameter is added in the image observation model to improve the results. The proposed algorithm is tested on simulated and real IKONOS images, and it results in improved image quality compared to other well-known methods in terms of both objective measurements and visual evaluation.

Index Terms—Compressed sensing (CS), image fusion, joint dictionary, tradeoff.

I. INTRODUCTION

WITH the rapid development of satellite sensors, remote sensing image data acquired by high-resolution optical sensors, such as IKONOS, QuickBird, and so on, have been widely used. Since the sensors have a physical tradeoff between the spatial and the spectral resolutions [1], [2], the acquired multispectral (MS) images often have coarser spatial resolution than the corresponding panchromatic (PAN) images. Pan-sharpening is a technique that artificially produces a high-resolution multispectral (HRM) image by fusing a high-resolution panchromatic (HRP) image and a low-resolution multispectral (LRM) image [3]. By the fusion of these images, we can overcome the limitations of information obtained from individual sources and obtain a better understanding of the observed scene [1], e.g., an HRM image offers more information than an LRM image for an urban area classification [4].

Manuscript received August 7, 2011; revised October 17, 2011; accepted November 8, 2011. Date of publication December 30, 2011; date of current version May 7, 2012. This work was supported in part by the National Basic Research Program of China (973 Program) under Grant 2011CB707105, by the National Natural Science Foundation of China under Grants 40930532, 41071269, and 40971220, by the Postdoctoral Science Foundation of China under Grant 2011M501242, by the State Key Laboratory of Information Engineering in Surveying, Mapping and Remote Sensing Special Research Funding, and by the Fundamental Research Funds for the Central Universities.

C. Jiang, H. Zhang, and L. Zhang are with the State Key Laboratory of Information Engineering in Surveying, Mapping, and Remote Sensing, Wuhan University, Wuhan 430079, China (e-mail: jiangcheng@whu.edu.cn; zhanghongyan@whu.edu.cn; zlp62@public.wh.hb.cn).

H. Shen is with the School of Resource and Environmental Science, Wuhan University, Wuhan 430079, China (e-mail: shenhf@whu.edu.cn).

Color versions of one or more of the figures in this paper are available online at <http://ieeexplore.ieee.org>.

Digital Object Identifier 10.1109/LGRS.2011.2177063

For more than two decades, a lot of image fusion algorithms have been proposed. Traditional projection-substitution-based methods include intensity–hue–saturation (IHS) [5], principal component analysis (PCA) [6], and Gram–Schmidt (GS) [7]. The Brovey transform [8], which belongs to the arithmetic-based methods, is another popular early algorithm. All the aforementioned methods are reported to have results with good spatial details but severe color distortions [8]. In the first decade of the 21st century, wavelet-based methods [9], [10] became well known for their reduced color distortions. They adopt the *amélioration de la résolution spatiale par injection de structures* (ARSIS) concept, which extracts details from the HRP image and injects the details using different strategies [10] into the LRM image. In the last few years, many model-based methods [1], [11], [12] have been proposed with better spatial and spectral performance than before.

Recently, Li and Yang [12] proposed a model-based method using a compressed sensing (CS) technique. Due to the advantages of the method in that it selects atom patches from the dictionary adaptively for each patch and those patches are the most relevant ones in the dictionary to represent the given LRM and HRP images, the reconstructed HRM images from the selected patches can satisfactorily preserve both the spatial and the spectral information of the source images [12]. In this method, HRM images with the same resolution as the desired fused image are used to construct the dictionary, which has proved to be applicable for simulated remote sensing images.

In view of this, we propose a practical CS-based pan-sharpening method. The contribution of this letter is twofold. First, we propose to construct a novel joint dictionary from both LRM and HRP training images, making the method applicable and practical for both simulated and real remote sensing images. Second, we adopt the observation model, which approximately views the LRM image as the decimation of the original HRM image and takes the HRP image as the linear combination of all bands of the HRM image. In our model, a tradeoff parameter, which balances the contribution of LRM and HRP for the final pan-sharpened results, is proposed to achieve better fusion results.

II. PAN-SHARPENING METHOD BASED ON CS

A. CS

In 2006, Candès *et al.* [13] and Donoho [14] proposed a new sparse sampling theory, namely, CS theory. A sparse signal is a signal that can be represented as a linear combination of relatively few base elements in a basis or an overcomplete dictionary. Studies have shown that such high-dimensional sparse signals can be accurately recovered from a drastically smaller

number of (even randomly selected) linear measurements [15]. The measurement process is written as

$$y = \Phi x = \Phi \Psi \alpha \quad (1)$$

where x is the vector of the original signal, Φ is referred to as the measurement matrix, and y is the vector of measurements. Ψ is the transform matrix or the so-called overcomplete dictionary that maps the sparse representation α into x .

Using measurements to recover the original signal is a reconstruction problem, and various methods have been investigated. Basis pursuit (BP) [16] may be the most well-known one, which views the reconstruction problem as an l_1 optimization problem formed as

$$\min \lambda \|\alpha\|_1 + \|y - \Phi \Psi \alpha\|_2^2 \quad (2)$$

where λ is called the regularization parameter. The main idea of BP is to convert (2) to the standard linear program, which is a mature technique at present. Other typical methods, like orthogonal matching pursuit and iteratively reweighted least squares, can be found in [17].

B. Pan-Sharpener Method Based on CS

First, we introduce the image observation model to relate the desired HRM image to both the observed LRM and HRP images, which is the prerequisite for the remote sensing image pan-sharpening method based on CS.

The degradation model between the LRM image and the HRM image is written as

$$y_{MS} = M_1 x + v_1 \quad (3)$$

where y_{MS} and x are column vectors (lexicographically ordering its pixels) representing the LRM image and the HRM image. M_1 is a matrix representing the blurring, the sensor integration function, and the spatial subsampling, and v_1 is the noise vector.

The linear model between the HRP image and each band image of HRM is as follows:

$$y_{PAN} = \sum_{b=1}^B w_b x_b + v_2 = M_2 x + v_2 \quad (4)$$

where column vector y_{PAN} represents the HRP image, w_b is the weight, and column vector x_b represents the b th band image of the HRM image. M_2 is the linear combination matrix, and v_2 is the noise vector.

We propose a tradeoff parameter β to combine (3) and (4) to form the observation model

$$y = Mx + v \quad (5)$$

where $y = \begin{bmatrix} y_{MS} \\ \beta y_{PAN} \end{bmatrix}$, $M = \begin{bmatrix} M_1 \\ \beta M_2 \end{bmatrix}$, and $v = \begin{bmatrix} v_1 \\ \beta v_2 \end{bmatrix}$. Here, the tradeoff parameter β is used to balance the contribution of LRM and HRP for the final pan-sharpened results. The detailed analysis will be given later.

From the perspective of CS, the observation model is similar to the measurement process. Thus, we take the HRM image as the original signal in the CS theory and assume that it is sparse in some image bases' space, and take LRM and HRP

images as measurements. Then, based on the CS reconstruction theory, a sparse representation of x can be adopted to solve the underdetermined observation model.

Assuming that the HRM image is sparse in a dictionary A , x can be expressed as

$$x = A\alpha \quad (6)$$

where α is a sparse vector with only a small number of nonzero components. Thus, using the sparse representation, the pan-sharpening model can be converted to an l_1 optimization problem formed by

$$\min \lambda \|\alpha\|_1 + \|y - MA\alpha\|_2^2 \quad (7)$$

BP is adopted to solve (7). After the optimal α is obtained, x can be recovered using (6).

In fact, (7) is equal to (8) as follows:

$$\min \lambda \|\alpha\|_1 + \left(\|y_{MS} - M_1 A\alpha\|_2^2 + \beta^2 \|y_{PAN} - M_2 A\alpha\|_2^2 \right) \quad (8)$$

The term $\|y_{MS} - M_1 A\alpha\|_2^2$ represents the data fidelity of the LRM image that provides a force of the conformance of the desired HRM image to the observed LRM image. The term $\|y_{PAN} - M_2 A\alpha\|_2^2$ provides a measure of the conformance of the HRM image to the HRP image. Therefore, the tradeoff β controls the relative contribution of LRM and HRP images to the overall cost function in (8). Observe that (5) is more general than the model in [12], which is just a special case of (5) with $\beta = 1$.

C. Joint Dictionary Construction

As we know, a good pan-sharpening result should make use of the spectral information of the LRM image and the spatial information of the HRP image as much as possible. Therefore, a simple idea is to use LRM and HRP training images to jointly construct the overcomplete dictionary. Then, with the l_1 optimization problem in (7), the most relevant spectral and spatial characteristics can be automatically extracted from the joint dictionary and combined to represent the HRM image.

The dictionary construction flowchart is shown in Fig. 1, which consists of four steps. The R, G, B, NIR, and PAN represent the red, green, blue, near-infrared, and panchromatic band images, respectively.

- 1) First, we get N training image pairs (N LRM images and N corresponding HRP images) and resample the LRM images to the same resolution as the HRP images, using cubic convolution in our experiments.
- 2) For the i th training image pair, we use all nonoverlapping $p \times p$ (p should be the same as the patch size of the HRM image discussed in Section II-D) raw patches of each LRM band image and the HRP image together as the i th samples and use the well-known dictionary training method, K-SVD [18], to obtain the i th trained dictionary A_i ($i = 1 : N$).
- 3) After all image pairs are trained separately, A_i are concatenated to get A_t , which is the trained dictionary of all N training image pairs

$$A_t = [A_1 \quad A_2 \quad \dots \quad A_N] \quad (9)$$

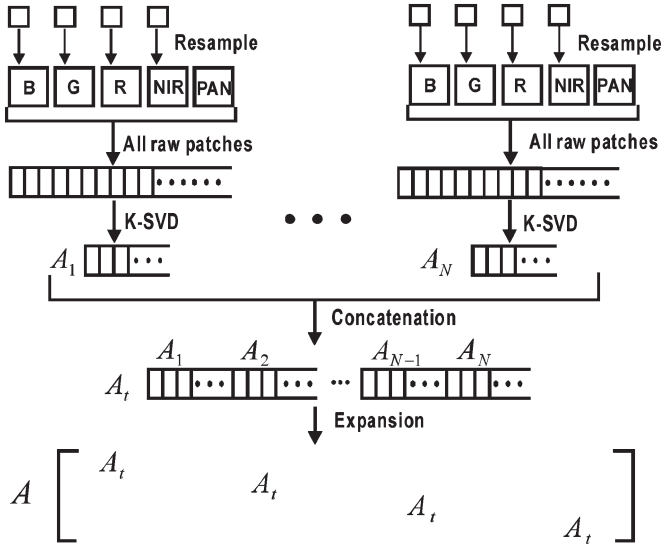


Fig. 1. Proposed dictionary construction flowchart.

Here, we train N training image pairs separately and then concatenate them, instead of training all the images together, mainly because of the concerns of the memory and computational complexity using K-SVD.

- 4) A_t is the trained dictionary in which each band of the fused HRM image is sparse. Since we process all the bands as a vector in our model, we expand A_t to A

$$A = \begin{bmatrix} A_t & & & \\ & A_t & & \\ & & A_t & \\ & & & A_t \end{bmatrix}. \quad (10)$$

With the dictionary A , the fused HRM image can be sparsely represented as

$$x = \begin{bmatrix} x_1 \\ x_2 \\ x_3 \\ x_4 \end{bmatrix} = \begin{bmatrix} A_t & & & \\ & A_t & & \\ & & A_t & \\ & & & A_t \end{bmatrix} \begin{bmatrix} \alpha_1 \\ \alpha_2 \\ \alpha_3 \\ \alpha_4 \end{bmatrix} = A\alpha. \quad (11)$$

D. Patch-Based Processing Strategy

Since BP and K-SVD cannot be applied to a large image directly [12], [18], [19], the proposed method is operated on image patches, as shown in Fig. 2. Based on the discussion in [19], the size of the image patch in the HRM is set as 8×8 , corresponding to 8×8 in the HRP image and 2×2 in the LRM image, as the spatial resolution ratio between the LRM image and the HRP image is 4. Therefore, the matrix M_1 in (3) is constructed as $(1/16) \cdot I_{8 \times 8} \otimes (1^T \otimes (I_{2 \times 2} \otimes 1^T))$, where $I_{N \times N}$ is an $N \times N$ identity matrix and 1 is a 4×1 vector with all entries equal to 1. The matrix M_2 in (4) is constructed as $(w_1 I \ w_2 I \ w_3 I \ w_4 I)$, where I is a 64×64 identity matrix. We process all patches in raster-scan order, from left-top to right-bottom with steps of one pixel in the LRM image and four pixels in the HRP image [12]. After all patches have been processed, the solution is averaged on the overlapped regions.

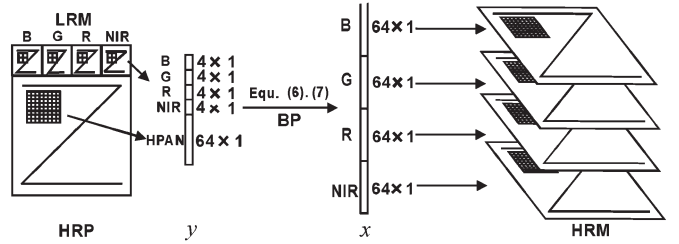


Fig. 2. Patch-based processing strategy.

III. EXPERIMENTS

To test the proposed method, we conduct both simulated experiments and real experiments using IKONOS images. In the simulated experiments, the 4-m resolution MS image and the 1-m resolution PAN image are degraded to a 16-m resolution MS image and a 4-m resolution PAN image, respectively, with low-pass filter and decimation operator by four to yield one, and then, pan-sharpening methods are selected to fuse them to a 4-m resolution MS image. Finally, we compare the fused MS image with the original HRM image to perform evaluations. We compare our method to fast IHS (FIHS) [5], GS [7], *à-trous* wavelet transform-based pan-sharpening (AWLP) [9], the method in [12], and the method in [12] improved with tradeoff. In the real experiments, we use the 4-m resolution MS image and the 1-m resolution PAN image directly to produce a 1-m resolution MS image. Due to the lack of 1-m resolution HRM training images, all the aforementioned methods are compared, except for the method in [12] and the method in [12] improved with tradeoff.

A. Simulated Experiments

The dictionary of the proposed method is constructed from 20 pairs of a degraded 16-m resolution MS image and its corresponding 4-m resolution PAN image. We degrade the training images with low-pass filter and decimation operator by four to yield one. The K-SVD parameter “EData,” the target error in L2-norm for coding each signal, is set as 100; the parameter “dictsize,” which represents the output dictionary size, is set as 1000; and the other parameters are set to default. Therefore, the A_t is a 64×1000 matrix. The λ in (7) is set as 1, around which the BP algorithm is stable. In (4), we set $w_1 = w_2 = w_3 = w_4 = 0.25$ with no bias. The tradeoff β in (5) is set empirically when most of the indexes reach their best performance. We use the following five quality indexes to conduct quantitative assessments: correlation coefficient (CC), root-mean-square error (RMSE), spectral angle mapper (SAM), *erreur relative globale adimensionnelle de synthèse* (ERGAS), and Q4.

Fig. 3 shows the fusion results. By visually comparing the fused images with the original HMS images, we can see that all the experimental methods can effectively pan-sharpen the LMS image data. However, the proposed method shows the best spectral preserving performance, for its color looks the most similar to the original HRM. On the whole, the proposed method not only provides high-quality spatial details but also satisfactorily preserves spectral information.

The quantitative assessment results are shown in Table I, in which the best results for each quality index are labeled in bold. The quantitative assessment results are consistent with the visual evaluations. It is observed that every index of the method

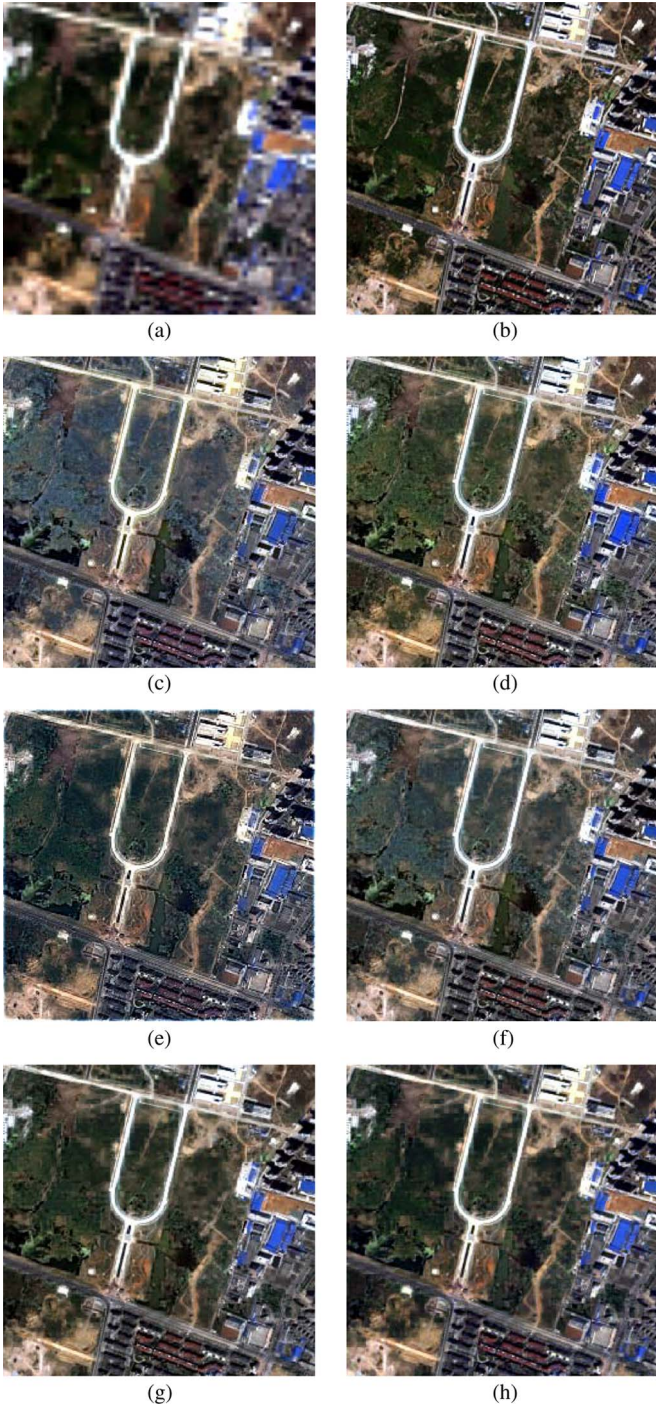


Fig. 3. Simulated experiment. (a) Resampled LRM (RGB, 256×256 , 16 m). (b) Original HRM (RGB, 256×256 , 4 m). (c) FIHS. (d) GS. (e) AWLP. (f) Method in [12]. (g) Method in [12] improved with tradeoff ($\beta = 0.25$). (h) Proposed method ($\beta = 0.0001$).

in [12] improved with the proposed tradeoff is better than that of the method in [12], which indicates the effectiveness and necessity of the proposed tradeoff parameter. From the table, we can see that except for the results of the method in [12] improved with the proposed tradeoff, the proposed method outperforms the existing methods in almost all the quality indexes.

The impact of β is investigated in Tables II and III, in which the best results for each quality index are labeled in bold. It

TABLE I
QUANTITATIVE ASSESSMENT RESULTS OF THE SIMULATED EXPERIMENT SHOWN IN FIG. 3. B, G, R, AND NIR REPRESENT THE RESULTS OF THE BLUE, GREEN, RED, AND NEAR-INFRARED BANDS, RESPECTIVELY, AND THE Avg IS THE AVERAGE RESULT AMONG THE RESULTS OF R, G, B, AND NIR

	FIHS	GS	AWLP	Method in [12]	[12] with $\beta=0.25$	Proposed $\beta=0.0001$
CC	B	0.8379	0.9344	0.8054	0.9175	0.9534
	G	0.9308	0.9412	0.8665	0.9474	0.9644
	R	0.9340	0.9348	0.9000	0.9460	0.9583
	NIR	0.9356	0.9200	0.8845	0.9464	0.9506
	Avg	0.9096	0.9326	0.8641	0.9393	0.9567
RMSE	B	56.8824	38.4283	68.6217	40.7694	28.1601
	G	56.6676	57.5907	78.3047	49.2114	38.0317
	R	67.1514	71.6315	76.4542	58.9317	49.7322
	NIR	76.8833	80.7587	98.1825	70.8442	64.0111
	Avg	64.3962	62.1023	80.3908	54.9392	44.9838
SAM	4.2737	4.1901	4.0331	3.5690	3.3830	
ERGAS	3.0821	2.9985	3.7871	2.6176	2.1526	
Q4	0.7576	0.7258	0.7055	0.8140	0.8212	

TABLE II
QUANTITATIVE ASSESSMENT RESULTS OF THE METHOD IN [12] IMPROVED WITH $\beta = 0.5^K$ (K IS FROM -1 TO 5) USING THE SAME DATA AS FIG. 3. CCavg AND RMSEavg REPRESENT THE AVERAGE RESULT AMONG ALL THE CC AND RMSE RESULTS OF ALL BANDS, RESPECTIVELY

K	-1	0	1	2	3	4	5
CCavg	0.9320	0.9393	0.9497	0.9567	0.9548	0.9379	0.9124
RMSEavg	58.1101	54.9392	49.1252	44.9838	46.2256	54.2457	63.4043
SAM	3.6619	3.5690	3.4799	3.3830	3.3429	3.4466	3.5974
ERGAS	2.7681	2.6176	2.3449	2.1526	2.2130	2.6010	3.0441
Q4	0.8108	0.8140	0.8202	0.8212	0.7913	0.7154	0.6346

TABLE III
QUANTITATIVE ASSESSMENT RESULTS OF THE PROPOSED METHOD WITH $\beta = 0.1^K$ (K IS FROM -1 TO 5) USING THE SAME DATA AS FIG. 3. CCavg AND RMSEavg REPRESENT THE AVERAGE RESULT AMONG ALL THE CC AND RMSE RESULTS OF ALL BANDS, RESPECTIVELY

K	-1	0	1	2	3	4	5
CCavg	0.9252	0.9431	0.9498	0.9500	0.9501	0.9556	0.9001
RMSEavg	59.7302	50.4690	46.9792	46.9611	46.9415	45.0035	67.4878
SAM	3.6645	3.5754	3.5524	3.5531	3.3551	3.4643	3.7093
ERGAS	2.8492	2.4061	2.2424	2.2416	2.2406	2.1580	3.2575
Q4	0.8105	0.8170	0.8191	0.8191	0.8192	0.8203	0.5909

shows that all the indexes vary with β and share the same trend, which improves gradually to the best but drops after the top value. Moreover, the best performance of every index is achieved at the same value of β , except for the SAM index, which is a little offset. It is observed that the optimal β in Table II is different from that in Table III, and the result of the proposed method is more robust to β . The reason for this is that they adopt different dictionaries. It should be noted that, even for the same method and for the same dictionary, the optimal β may vary from different experimental images. How to determine β automatically and precisely is still an open problem and needs further investigation.

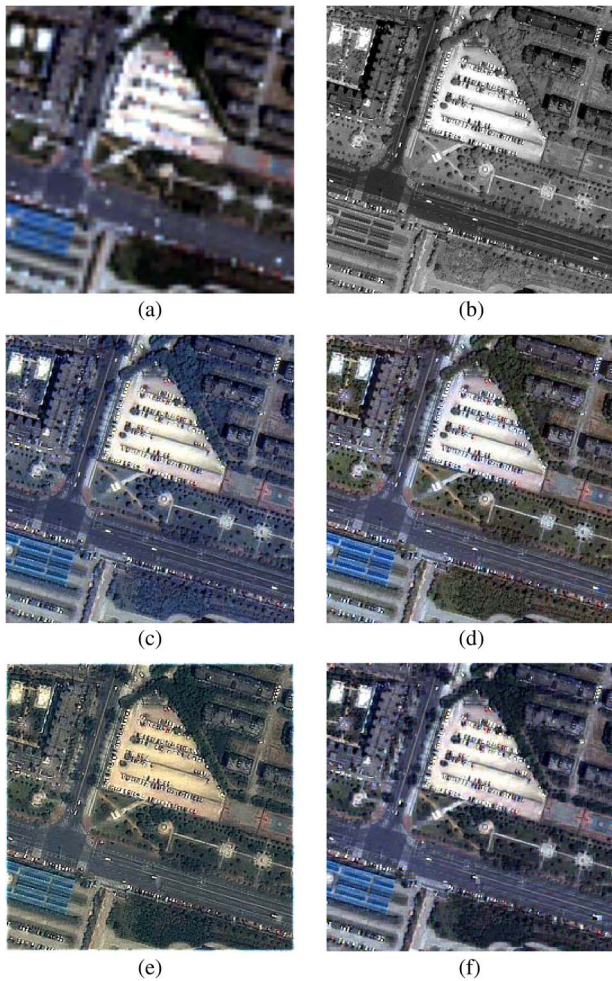


Fig. 4. Real experiment. (a) Resampled LRM (RGB, 256×256 , 4 m). (b) HRP (256×256 , 1 m). (c) FIHS. (d) GS. (e) AWLP. (f) Proposed method ($\beta = 0.0001$).

B. Real Experiments

The dictionary of the proposed method is constructed from 20 pairs of a 4-m resolution MS image and its corresponding 1-m resolution PAN image. The tradeoff parameter β is set as 0.0001 empirically, and the results are shown in Fig. 4. This shows that the proposed method achieves both visually good spatial and spectral effects. Moreover, we found that the GS result is also good visually. The difference between the GS result and the proposed method is that the GS result is brighter, particularly in vegetation areas, so GS is good for visual interpretation. However, from Wald's protocol [20] that any synthetic image should be as identical as possible to the image that the corresponding sensor would observe with the highest spatial resolution, the proposed method shows significant advantages.

IV. CONCLUSION

This letter proposes a new CS-based image fusion method, which is applicable, in practice, to fuse real remote sensing images by constructing a joint dictionary from HRP and LRM images. To improve the effectiveness, a tradeoff parameter is

also proposed in the observation model. The proposed method is compared with the typical FIHS, GS, AWLP methods, and the state-of-the-art method in [12]. The experimental results suggest that the proposed method can achieve competitive spatial quality compared to the other well-known methods and recover most of the spectral information that the corresponding sensor would observe with the highest spatial resolution.

REFERENCES

- [1] M. V. Joshi, L. Bruzzone, and S. Chaudhuri, "A model-based approach to multiresolution fusion in remotely sensed images," *IEEE Trans. Geosci. Remote Sens.*, vol. 44, no. 9, pp. 2549–2562, Sep. 2006.
- [2] L. Zhang, H. Zhang, H. Shen, and P. Li, "A super-resolution reconstruction algorithm for surveillance images," *Signal Process.*, vol. 90, no. 3, pp. 848–859, Mar. 2010.
- [3] Y. Mitani and Y. Hamamoto, "A consideration of pan-sharpen images by HSI transformation approach," in *Proc. SICE Ann. Conf.*, 2010, pp. 1283–1284.
- [4] X. Huang, L. Zhang, and P. Li, "Classification and extraction of spatial features in urban areas using high-resolution multispectral imagery," *IEEE Geosci. Remote Sens. Lett.*, vol. 4, no. 2, pp. 260–264, Apr. 2007.
- [5] T.-M. Tu, P. S. Huang, C.-L. Hung, and C.-P. Chang, "A fast intensity-hue-saturation fusion technique with spectral adjustment for IKONOS imagery," *IEEE Geosci. Remote Sens. Lett.*, vol. 1, no. 4, pp. 309–312, Oct. 2004.
- [6] P. S. Chavez, Jr., S. C. Sides, and J. A. Anderson, "Comparison of three different methods to merge multiresolution and multispectral data: Landsat TM and SPOT panchromatic," *Photogramm. Eng. Remote Sens.*, vol. 57, pp. 295–303, 1991.
- [7] C. A. Laben, V. Bernard, and W. Brower, "Process for enhancing the spatial resolution of multispectral imagery using pan-sharpening," U.S. Patent 6 011 875, Jan. 4, 2000.
- [8] Y. Zhang, "Problems in the fusion of commercial high-resolution satellite images as well as LANDSAT 7 images and initial solutions," *Proc. GeoSpatial Theory, Process. Appl.*, vol. 34, pt. 4, pp. 9–12, 2002.
- [9] X. Otazu, M. González-Audicana, O. Fors, and J. Núñez, "Introduction of sensor spectral response into image fusion methods. Application of wavelet-based methods," *IEEE Trans. Geosci. Remote Sens.*, vol. 43, no. 10, pp. 2376–2385, Oct. 2005.
- [10] K. Amolins, Y. Zhang, and P. Dare, "Wavelet based image fusion techniques—An introduction, review and comparison," *ISPRS J. Photogramm. Remote Sens.*, vol. 62, no. 4, pp. 249–263, Sep. 2007.
- [11] M. Joshi and A. Jalobeanu, "MAP estimation for multiresolution fusion in remotely sensed images using an IGMRF prior model," *IEEE Trans. Geosci. Remote Sens.*, vol. 48, no. 3, pp. 1245–1255, Mar. 2010.
- [12] S. Li and B. Yang, "A new pan-sharpening method using a compressed sensing technique," *IEEE Trans. Geosci. Remote Sens.*, vol. 49, no. 2, pp. 738–746, Feb. 2011.
- [13] E. Candès, J. Romberg, and T. Tao, "Robust uncertainty principles: Exact signal reconstruction from highly incomplete frequency information," *IEEE Trans. Inf. Theory*, vol. 52, no. 2, pp. 489–509, Feb. 2006.
- [14] D. L. Donoho, "Compressed sensing," *IEEE Trans. Inf. Theory*, vol. 52, no. 4, pp. 1289–1306, Apr. 2006.
- [15] R. G. Baraniuk, E. Candès, M. Elad, and Y. Ma, "Applications of sparse representation and compressive sensing," *Proc. IEEE*, vol. 98, no. 6, pp. 906–909, Jun. 2010.
- [16] S. Chen, D. Donoho, and M. Saunders, "Atomic decomposition by basis pursuit," *SIAM Rev.*, vol. 43, no. 1, pp. 129–159, 2001.
- [17] A. Bruckstein, D. Donoho, and M. Elad, "From sparse solutions of systems of equations to sparse modeling of signals and images," *SIAM Rev.*, vol. 51, no. 1, pp. 34–81, Jan. 2009.
- [18] M. Aharon, M. Elad, and A. M. Bruckstein, "The K-SVD: An algorithm for designing of overcomplete dictionaries for sparse representations," *IEEE Trans. Image Process.*, vol. 54, no. 11, pp. 4311–4322, Nov. 2006.
- [19] B. Yang and S. Li, "Multifocus image fusion and restoration with sparse representation," *IEEE Trans. Instrum. Meas.*, vol. 59, no. 4, pp. 884–892, Apr. 2010.
- [20] L. Wald, T. Ranchin, and M. Mangolini, "Fusion of satellite images of different spatial resolution: Assessing the quality of resulting images," *Photogramm. Eng. Remote Sens.*, vol. 63, no. 6, pp. 691–699, Jun. 1997.